

**The Henryk Niewodniczański  
INSTITUTE OF NUCLEAR PHYSICS  
Polish Academy of Sciences  
ul. Radzikowskiego 152, 31-342 Kraków, Poland**

www.ifj.edu.pl/publ/reports/2014/

Kraków, 2014

---

**Report No. 2074/AP**

**Physical assumptions for a design of the DET-12  
chamber for detection of delayed neutrons**

*Barbara Bieńkowska<sup>1</sup>, Krzysztof Drozdowicz<sup>2</sup>, Barbara Gabańska<sup>2</sup>,  
Andrzej Igielski<sup>2</sup>, Rafał Prokopowicz<sup>1,3</sup>, Urszula Wiącek<sup>2</sup>, Urszula Woźnicka<sup>2</sup>*

<sup>1</sup>Institute of Plasma Physics and Laser Microfusion, ul. Hery 23, 01-497 Warsaw, Poland

<sup>2</sup>Institute of Nuclear Physics PAN, ul. Radzikowskiego 152, 31-342 Kraków, Poland

<sup>3</sup>National Centre for Nuclear Research, ul. A. Sołtana 7, 05-400 Otwock-Świerk, Poland

The work has been partly performed within the framework of the strategic research project “Technologies supporting development of safe nuclear power engineering” financed by the National Centre for Research and Development (NCBiR). Research task „Research and development of techniques for the controlled thermonuclear fusion”, Contract No. SP/J/2/143234/11.

**Abstract**

Physical assumptions have been outlined to design a new device (DET-12) for measurements of delayed neutron emitted from samples of fissionable materials activated with neutrons at big fusion-plasma devices. The aim is to support in this way a classic neutron activation method used as one of the hot plasma diagnostics at tokamaks or stellarators. Physical fundamentals of generation of the delayed neutrons are mentioned and a resulting concept of the measuring chamber is presented. A general size and dimensions of particular constituent material layers, and a number and placement of neutron detectors are optimized by means of Monte Carlo modelling of the neutron transport. Recommendations for a technical design of the measuring chamber are formulated.



## 1. Introduction

One of the most accurate neutron measurement method for fusion plasma diagnostics is neutron activation of purpose-selected materials. Samples of chosen nuclides are placed in exposition locations, close to the plasma or spread in the fusion device hall. They are irradiated by neutrons coming from the D-D or D-T reactions. After the activation the samples are quickly delivered with a pneumatic transport system to a gamma-ray spectrometer. Measured activity allows to determine neutron field properties. The method allows absolute determination of neutron flux density when energy spectrum is known. It also allows to verify neutron spectrum prediction (benchmark against numerical or analytical calculations) or to establish the spectrum, based on tentative assumptions (spectrum deconvolution). The method consists in irradiation of materials with neutron reaction cross-section suitable for examined neutron field. By measuring the neutron reaction products the neutron field properties, *i.e.* flux density and/or energy spectrum is deconvoluted (restored). The method is free from mechanical, electrical and magnetic interferences.

A valuable supplement to this method is the irradiation (the neutron activation) of fissile or fissionable materials. Following, the fission products are recorded by identifying their characteristic  $\gamma$ -radiation (by means of  $\gamma$ -spectrometry). Alternatively, they can be recorded overall by measuring characteristic decay of beta-delayed neutron emission.

The first mentioned above approach, using  $\gamma$ -spectrometry, is usually long-lasting and laborious. Besides, efficiency of  $\gamma$ -radiation recording with high energy resolution is relatively low. Whereas, recording of the neutrons emitted from irradiated sample is usually much faster and its automation is straightforward. The beta-delayed neutrons are easy for detection. Such measurements are less sensitive to the background radiation, as well.

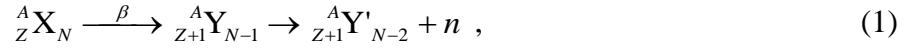
### 1.1. Physical fundamentals

Delayed neutrons are emitted from unstable, neutron-rich atomic nuclei. Such delayed neutron emitter is usually a product of  $\beta$ -decay of other neutron-rich nucleus, called the delayed neutron precursor. Far from stable nuclei the precursor decay energies may be large enough to populate highly excited states of the emitter. If energy of such state is higher than the neutron separation (binding) energy then neutron emission can be more probable than following  $\beta$  or  $\gamma$  transition. Neutron emission occurs in  $10^{-12} - 10^{-16}$  s (like other nuclear transitions), and thus overall neutron emission occurs with half-life characteristic to the precursor  $\beta$ -decay [1]. If the precursor is a fission product (a fission fragment) then the emitted neutron is called “delayed neutron”, because it does not appear immediately, after fission itself. The prompt neutrons are emitted  $10^{-14} - 10^{-16}$  s after fission, whereas emission of the delayed neutrons from fission products occurs from milliseconds up to minutes later. Commonly, six distinct groups of emitters half-lives were recognized [2]. In recent years,

eight groups are distinguished [3] although they do not alter essentially the overall time behavior of the decay. Delayed neutrons are only a small fraction of all neutrons emitted during fission, *e.g.* below 0.7% for  $^{235}\text{U}$ .

Neutron emission competes to other nuclear transitions, mostly  $\gamma$ . Thus, from the same emitter, neutrons with various energies can be emitted connected with the emitter excited states energies. Beside of that, the emitters of two or even three delayed neutrons have been found.

The decay chain can be generally written as:



where the X nucleus is the delayed neutron precursor and Y is the delayed neutron emitter.

The delay is determined by the half-life of the precursor. As mentioned, a number of groups of the delayed neutrons (originated by different fission products) is distinguished and the total decay in time is described by:

$$S(t) = r_f \sum_{i=1}^G v_{di} \lambda_{di} \exp(-\lambda_{di} t) , \quad (2)$$

where  $r_f$  is the number of fission reactions in the sample,  $v_{di}$  is the yield of the  $i$ -th delayed neutron group,  $\lambda_{di}$  is the decay constant of this group, and  $G$  is the number of groups. The corresponding half-life can range in some cases up to 1 or 2 minutes. For example, the  $^{235}\text{U}$  fission products being the precursors for the delayed neutrons, have the average half-lives from  $\sim 0.2$  s to  $\sim 56$  s.

The activated samples can be transported in the same pneumatic (or another) system as used for the activation measurements, to a different detection assembly. When the relevant fission cross-sections (for production of the X precursors) are known with a high accuracy as well as the X half-lives, the recorded time distributions  $S(t)$  of the delayed neutrons bring valuable information on the primary neutron field(s) [4]. Some problems can arise during the calculations because of insufficient or inaccurate nuclear data for neutron reactions with particular isotopes. New libraries are being extensively created and developed. For example, the recent version of the JEFF-3.1 [5], [6] contains, among others, the fission yield library for 19 isotopes and the thermal scattering law library for 9 materials [7]. A new issue of the US evaluation, the ENDF/B-VII.0 library, is recently released.

## 1.2. Delayed neutron diagnostics on JET tokamak

The activation method using delayed neutrons have been successfully applied in large fusion devices (tokamaks). Unlike the fissile materials, the fissionable ones have energy threshold cross-section for fission induced by fast neutron. The fissionable materials instead

of fissile ones are, therefore, usually used in case of fusion diagnostics (2.45 or 14 MeV neutrons).

The standard activation method based on  $\gamma$ -spectrometry is used in JET tokamak together with the method based on delayed neutrons. Both diagnostics are connected to the same pneumatic rabbit system to deliver capsules with activation samples to the tokamak and, after irradiation, to retrieve them back to the counting system, i.e.  $\gamma$ -spectrometers or helium counters respectively. There are seven irradiation ends located just outside the tokamak vacuum vessel and one located inside the vessel. It has to be, therefore, cooled-down by water in order to prevent melting of the polyethylene capsule.

Unlike the indium used in  $\gamma$ -spectrometry based activation method, the fissionable samples can be irradiated in each plasma discharge, one after another, due to short half-lives of delayed neutron precursors.

The main reason of using (both) activation techniques at JET is cross-calibration of others neutron diagnostics. The activation diagnostics are the only which can be directly calibrated by means of radioactive source. As a fissionable activation material  $^{232}\text{Th}$  is currently used at JET. Previously,  $^{238}\text{U}$  has also been used, but initially  $^{226}\text{Ra}$ ,  $^{234}\text{Th}$ ,  $^{231}\text{Pa}$ ,  $^{235}\text{U}$ ,  $^{237}\text{Np}$ ,  $^{239}\text{Pu}$  and  $^{241}\text{Am}$  have been considered as well [8].

Two delayed neutron counter assemblies are used. Each of them consists of a polythene moderator (40 cm in diameter) in which is embedded end of the rabbit system, to which a capsule can be transferred after irradiation. Six  $^3\text{He}$  proportional counters (one inch diameter, 15 cm sensitive length) surround the transport system end (at a radial distance of 8 cm), forming a hexagonal array. The whole system is protected against background neutrons by means of a 1 mm thick Cd screen and a 10 cm thick polyethylene shield [9]. In the treatment of the  $^{238}\text{U}$  measurements, the 18% contribution of the small  $^{235}\text{U}$  contamination (0.4%) has been taken into account. The detection efficiency has been established to be  $(14.6 \pm 0.28) \%$  for  $^{238}\text{U}$ . Difference in the detection efficiency in case of  $^{238}\text{U}$  and  $^{232}\text{Th}$  have been found due to differences in energies of the emitted neutrons [10].

In the frame of many experiments at JET it has been found that together with suitable neutron transport calculations the delayed neutron method gives more accurate results for the measured neutron fluences than does the use of indium [11].

## 2. Conceptual design of a new device to measure delayed neutrons

In order to prepare the activation measurements by means of delayed-neutron method a suitable measuring set-up has been designed. The Proportional counters filled-in with  $^3\text{He}$  have been chosen for detection of delayed neutrons [12]. The counters detect the neutrons through the following nuclear reaction:  $^3\text{He} + n \rightarrow ^3\text{H} + p$ . Due to an extremely high reaction cross-section for thermal neutrons (ca. 5000 barn) it was decided to slow-down (thermalize) the fast neutrons coming from  $\beta$ -decay precursors. The delayed neutron energy spectrum is similar to

the one of prompt neutrons but much softer. It slightly depends on initial energy of the fission neutron and can be approximated by the Maxwellian distribution with average energies roughly in the 400 to 600 keV range. Therefore, a suitable moderator layer is needed to slow-down fast neutrons. The measuring set-up need to be shielded from background neutrons by material with high-enough absorption cross-section. The detectors should have low gamma-ray sensitivity.

The shape of the measuring device has been taken as a parallelepiped with the square cross-section (Fig. 1). A chamber for the measured sample (which emits the delayed neutrons) is surrounded by a bismuth layer which prevents the accompanied  $\gamma$  radiation enter the detectors. The next layer is made of polyethylene and contains neutron detectors. Fast neutrons are slowed down in polyethylene and thermal neutrons are recorded by the  $^3\text{He}$  detectors. This part of the device is surrounded by layers which prevent outside background neutrons enter the measuring chamber. Looking from outside, it consists of borated polyethylene, cadmium, and a  $\text{B}_4\text{C}$  layers. Polyethylene with boron slows down external fast neutrons and partly absorbs the resulting thermal neutrons. Any remaining thermal neutrons are absorbed by cadmium and finally in the layer of boron carbide.

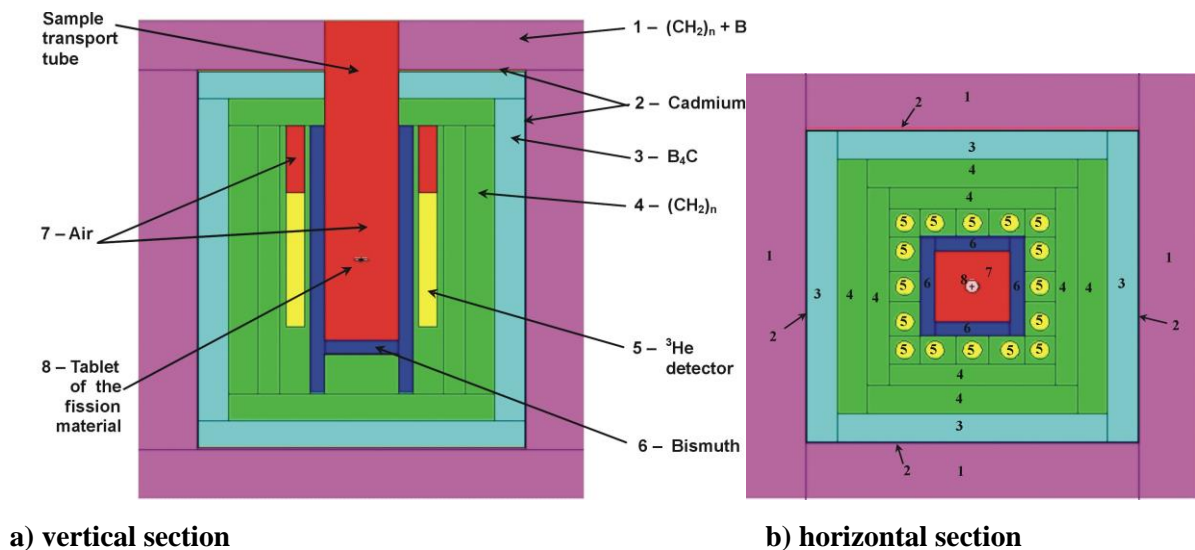


**Fig. 1.** Schematic cross section of the setup for the delayed neutron detection.

For creation of a basic model for the radiation transport through the mentioned layers, the following preliminary sizes have been assumed:

- total width = length = 60.4 cm,
- total height = 72.4 cm,
- outer layer of borated polyethylene (No.1), width = 8 cm,
- cadmium layer (No.2), width = 0.2 cm,
- boron carbide layer (No.3), width = 4 cm,

polyethylene layer (No.4) with neutron detectors, width at sides = 7 cm,  
width at top and bottom = 4 cm,  
bismuth layer (No.6), width = 2 cm,  
transport tube opening = 10 cm × 10 cm.

### 3. Optimisation of the device dimensions

Preliminary assumptions for the device for detection of delayed neutrons have been formulated. An initial important part of the research before designing the device has been performed by a computer simulation method. The numerical simulations have been made using the Monte Carlo method for calculation of the transport of neutrons (and other particles) in the matter. The MCNP code [13], [14] has been used for this purpose. Essential stages of the physical effects have been modelled, including geometry of the device, nuclear reactions in the activated tablets of fissionable materials, slowing-down and transport of neutrons through consecutive layers of the device to the neutron detectors, and detection of thermal neutrons.

The series of simulations were performed to define the efficiency of the delayed neutron detection. The transport of neutrons from the activated sample to the  $^3\text{He}$  detectors was modelled and the absorption events in the detectors were counted.

Two approximations were considered:

(i) Closer to the reality:

- fast neutrons are generated in the volume of the activated sample and initialize fission reactions,
- the prompt and delayed neutrons appear,
- transport through the components of the device is modelled and the number of neutron absorptions in the detectors is counted after 10 seconds;

(ii) More simplified (to speed up the calculation):

- delayed neutrons of the known energy distribution are emitted from the activated sample volume,
- the thermal neutrons are counted like in method (i).

The efficiency was defined as the ratio of the neutrons observed in the detectors (as a number of the absorption reactions) to the number of neutrons leaving the activated sample.

The calculations with method (i) were performed to get the reference results and to obtain the energy distributions of the delayed neutrons emitted after fissions in selected isotopes. The energy spectra are shown in Fig. 2.

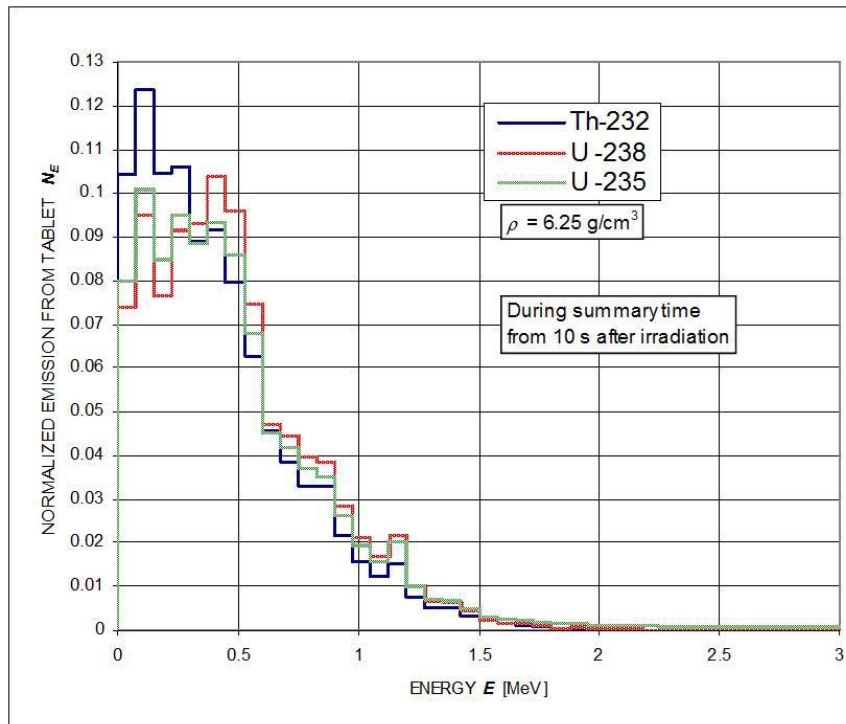


**Fig. 2.** Calculated energy spectra of delayed neutrons.

Results obtained with method (ii) were compared to those from simulation (i). For 16 detectors in layer No.4 only statistical differences were observed. and the computer simulation (ii) was a few thousand times faster. Thus, the method to generate in the activated sample volume directly neutrons of a respective energy distribution was accepted for energy-spatial simulations of the transport.

The device parameters were optimised by performing certain MCNP simulations. The influence of a number of detectors or particular device dimensions on the detection efficiency was investigated.

### 3.1. Borated polyethylene layer

Considering thickness of the outer borated polyethylene layer the worst possible situation was assumed in the simulations. The measuring device was irradiated from all sides with thermal neutrons, the sample transport tube was opened. A scheme is shown in Fig. 3. The neutron source was assumed as a spherical surface (70 cm radius) surrounding the device. Thermal neutrons of the Maxwellian energy distribution with the most probable energy  $E_T = 25.3 \times 10^{-3} \text{ eV}$  were emitted.



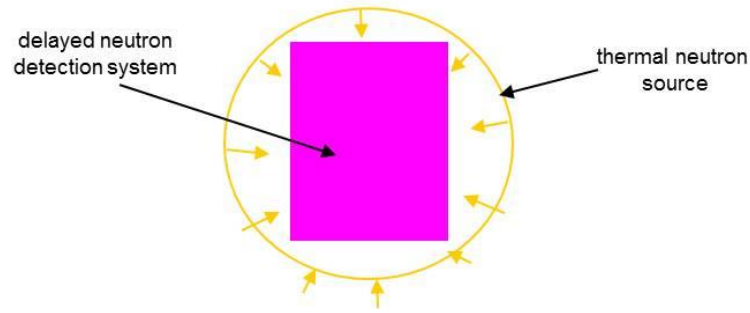


**Fig. 3.** Scheme of the delayed neutron detection system placed in the external thermal neutron field.

In this case, the borated polyethylene layer was optimized in respect to its width and to the boron content. The results for each detector are presented in Tables 1a and 1b. A summary plot is shown in Fig. 4. The number of recorded outer neutrons decreases significantly when 5 wt.% of boron is added to the protecting polyethylene. A further increase of boron amount, even so much as to 25%, brings only a very weak effect.

**Table 1a.** Detection of outer thermal neutrons in the device with 4 cm polyethylene protection layer ( $N$  – number of detected neutrons per 1 source neutron,  $\delta(N)$  – relative error).

Detector No.	without boron		5% boron concentration		25% boron concentration	
	$N$	$\delta(N)$	$N$	$\delta(N)$	$N$	$\delta(N)$
1	2.01E-08	0.057	1.60E-08	0.0637	1.44E-08	0.0673
2	7.83E-08	0.033	6.22E-08	0.0375	5.90E-08	0.0387
3	9.50E-08	0.0288	7.48E-08	0.0326	6.92E-08	0.0337
4	8.60E-08	0.0323	6.55E-08	0.0366	6.11E-08	0.0375
5	2.10E-08	0.0573	1.63E-08	0.0661	1.52E-08	0.0689
6	8.01E-08	0.0316	6.34E-08	0.0362	5.90E-08	0.0375
7	8.48E-08	0.0325	6.64E-08	0.0366	6.22E-08	0.0381
8	9.84E-08	0.0296	7.69E-08	0.0334	7.19E-08	0.0348
9	9.87E-08	0.0296	7.77E-08	0.034	7.37E-08	0.0351
10	8.00E-08	0.0326	6.40E-08	0.0373	5.99E-08	0.0388
11	8.47E-08	0.0314	6.76E-08	0.036	6.37E-08	0.0373
12	2.30E-08	0.0566	1.74E-08	0.0661	1.67E-08	0.0681
13	8.12E-08	0.0323	6.38E-08	0.0366	6.01E-08	0.0379
14	1.01E-07	0.0295	7.88E-08	0.034	7.36E-08	0.035
15	8.24E-08	0.0318	6.59E-08	0.0364	6.18E-08	0.0376
16	2.27E-08	0.0573	1.84E-08	0.0658	1.73E-08	0.0683
Total	1.15E-04	0.0089	9.07E-05	0.0101	8.50E-05	0.0105

**Table 1b** Detection of outer thermal neutrons in the device with 8 cm polyethylene protection layer

( $N$  – number of detected neutrons per 1 source neutron,  $\delta(N)$  – relative error).

Detector No.	without boron		5% boron concentration		25% boron concentration	
	$N$	$\delta(N)$	$N$	$\delta(N)$	$N$	$\delta(N)$
1	1.16E-08	0.0749	7.36E-09	0.0915	6.08E-09	0.0994
2	4.80E-08	0.0417	3.06E-08	0.0522	2.72E-08	0.0538
3	5.61E-08	0.0381	3.61E-08	0.0477	3.24E-08	0.0506
4	4.93E-08	0.0417	3.34E-08	0.0531	3.08E-08	0.056
5	1.37E-08	0.0728	9.85E-09	0.0863	8.06E-09	0.0932
6	4.68E-08	0.0414	3.13E-08	0.0522	2.83E-08	0.0545
7	4.33E-08	0.0444	2.80E-08	0.0562	2.56E-08	0.059
8	5.40E-08	0.0396	3.53E-08	0.051	3.19E-08	0.0541
9	5.41E-08	0.039	3.68E-08	0.0482	3.36E-08	0.0511
10	4.31E-08	0.0434	2.87E-08	0.0555	2.56E-08	0.0592
11	4.50E-08	0.0422	3.09E-08	0.0535	2.78E-08	0.0564
12	1.21E-08	0.0745	7.23E-09	0.0975	6.30E-09	0.104
13	4.45E-08	0.0425	2.93E-08	0.0533	2.67E-08	0.0562
14	5.34E-08	0.0386	3.44E-08	0.0493	3.07E-08	0.0521
15	4.76E-08	0.0414	3.22E-08	0.0522	2.95E-08	0.0546
16	1.18E-08	0.0725	7.74E-09	0.0933	7.03E-09	0.0987
Total	6.43E-05	0.0117	4.25E-05	0.0148	3.82E-05	0.0156

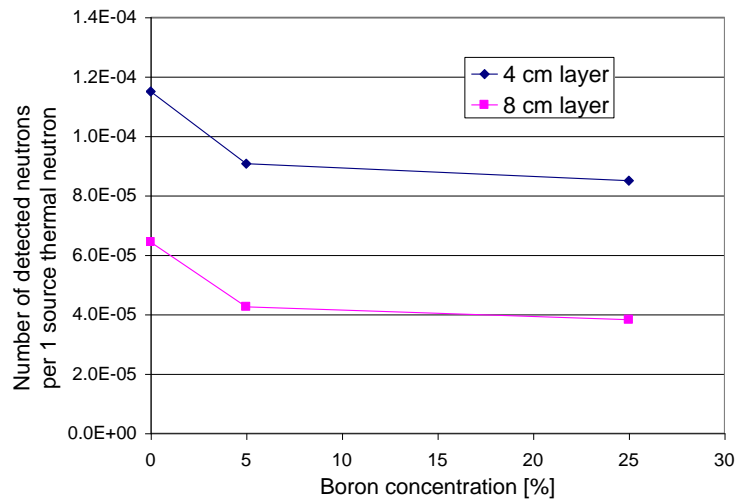


**Fig. 4.** Effectiveness of the polyethylene protection layer as a function of the boron content.

### 3.2. Number of the $^3\text{He}$ detectors

The total efficiency of detection was calculated as a sum from all detectors. A part of the device with numbered positions of the detectors is shown in Fig. 5. The simulations were performed when all 16 detectors were accounted and when 12 detectors were used, *i.e.* when the detectors in corners (#1, #5, #12, and #16) were removed. The results are presented in Tables 2a and 2b. As expected, the contribution of the corner detectors is smaller than of the others. A decrease of the efficiency, ratio  $\epsilon(N_{12})/\epsilon(N_{16}) \approx 0.87$ , is smaller than that which would result from the ratio of numbers of the detectors,  $12/16 = 0.75$ . It is justified to conclude that 12 detectors should be enough to ensure efficient neutron detection.

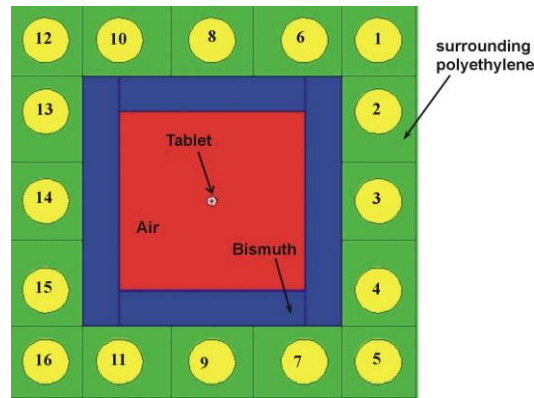


**Fig. 5.** Numbering of the  $^3\text{He}$  detectors in the detecting device.

**Table 2a.** Total efficiency of detection of delayed neutrons from  $^{235}\text{U}$  in the assembly of the  $^3\text{He}$  detectors.

Activated $^{235}\text{U}$ sample		Detection efficiency $\epsilon$ [%]		Efficiency ratio $\epsilon(N_{12})/\epsilon(N_{16})$
Mass [g]	Size $2r \times h$ [cm]	16 detectors	12 detectors	
1.5	$0.54 \times 1.51$	24.0	21.3	0.89
4	$1.8 \times 0.25$	35.4	30.5	0.86
11	$0.54 \times 1.51$	23.2	20.5	0.88

**Table 2b.** Total efficiency of detection of delayed neutrons from  $^{232}\text{Th}$  in the assembly of the  $^3\text{He}$  detectors.

Activated $^{232}\text{Th}$ sample		Detection efficiency [%]		Efficiency ratio $\epsilon(N_{12})/\epsilon(N_{16})$
Mass [g]	Size $2r \times h$ [cm]	16 detectors	12 detectors	
1.5	$0.96 \times 1.51$	26.4	21.6	0.82
4	$1.8 \times 0.25$	36.5	32.6	0.89
11	$0.96 \times 1.51$	25.7	21.8	0.85

### 3.3. Placement of the $^3\text{He}$ detectors

The thicker is the moderator layer the higher is efficiency of moderating the neutrons. But the longer is neutron path in the moderator the stronger is absorption and higher is number of unprofitable scatterings (escape of neutrons outside the layer or a longer travel path). A width of the layer behind the detector also influences the detection acting still as the moderator and also as the reflector of neutrons.

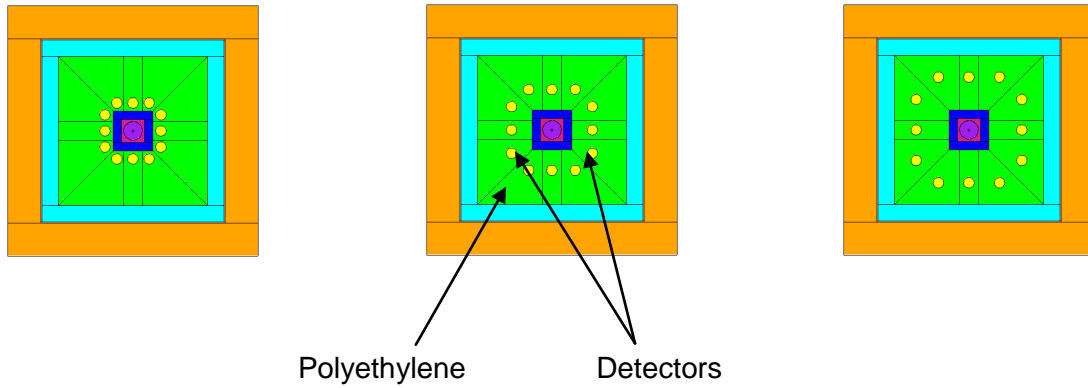


**Fig. 6.** Varying arrangement of the  $^3\text{He}$  detectors.

The boundary between the bismuth and polyethylene layers has been taken as a reference point for definition of a depth of the detector position,  $d$ , inside the layer. Series of simulations of the neutron transport have been made. The distance  $d$  of the detector axis from this inner boundary surface has been varied from 2 to 10 cm. Typical  $^3\text{He}$  detectors have been considered: a 1 inch diameter, a 25 cm active length and a 5 atm. pressure. An idea of the changing arrangement is shown in Fig. 6 (Nine arrangements in total have been studied). The activated sample has been always located in the centre. It has been used as the neutron source (of defined energy and time distributions, as shown above). Number of detections, *i.e.* neutron absorptions, in the detector volume has been tested. The simulations have been performed for the sizes of the inner hole equal to  $5 \times 5 \text{ cm}^2$  and  $10 \times 10 \text{ cm}^2$ . Examples of the results are shown in Fig. 7. A hole which is too large diminishes significantly the detector signal although an optimum position of the detector remains almost the same. Due to the technical reasons it seems that a sufficient space for the pneumatic transport ending will be closer to  $5.5 \times 5.5 \text{ cm}^2$ . The final modelling of the neutron transport has been performed for this size, using the fissionable material samples ( $^{232}\text{Th}$ ,  $^{235}\text{U}$ ,  $^{238}\text{U}$ ) shaped as cylinders of the diameter  $2r = 4.5 \text{ cm}$  and the height  $h = 1 \text{ cm}$ , of density  $\rho = 6.25 \text{ g/cm}^3$ . Plots of the results are shown in Figs. 8 and 9. “Total detector relative signal  $N$ ” means a summary signal from all detectors. The relative signal is the number of neutron counts, *i.e.* the number of neutron absorptions in the active volume of the detector, expressed as a fraction per one source neutron, as usual in the MCNP calculations.

Computer modelling allows us, of course, to investigate also the behaviour of neutrons immediately after the irradiation is finished and, thus, to observe an influence of the mentioned few-second's delay necessary for the sample transport.

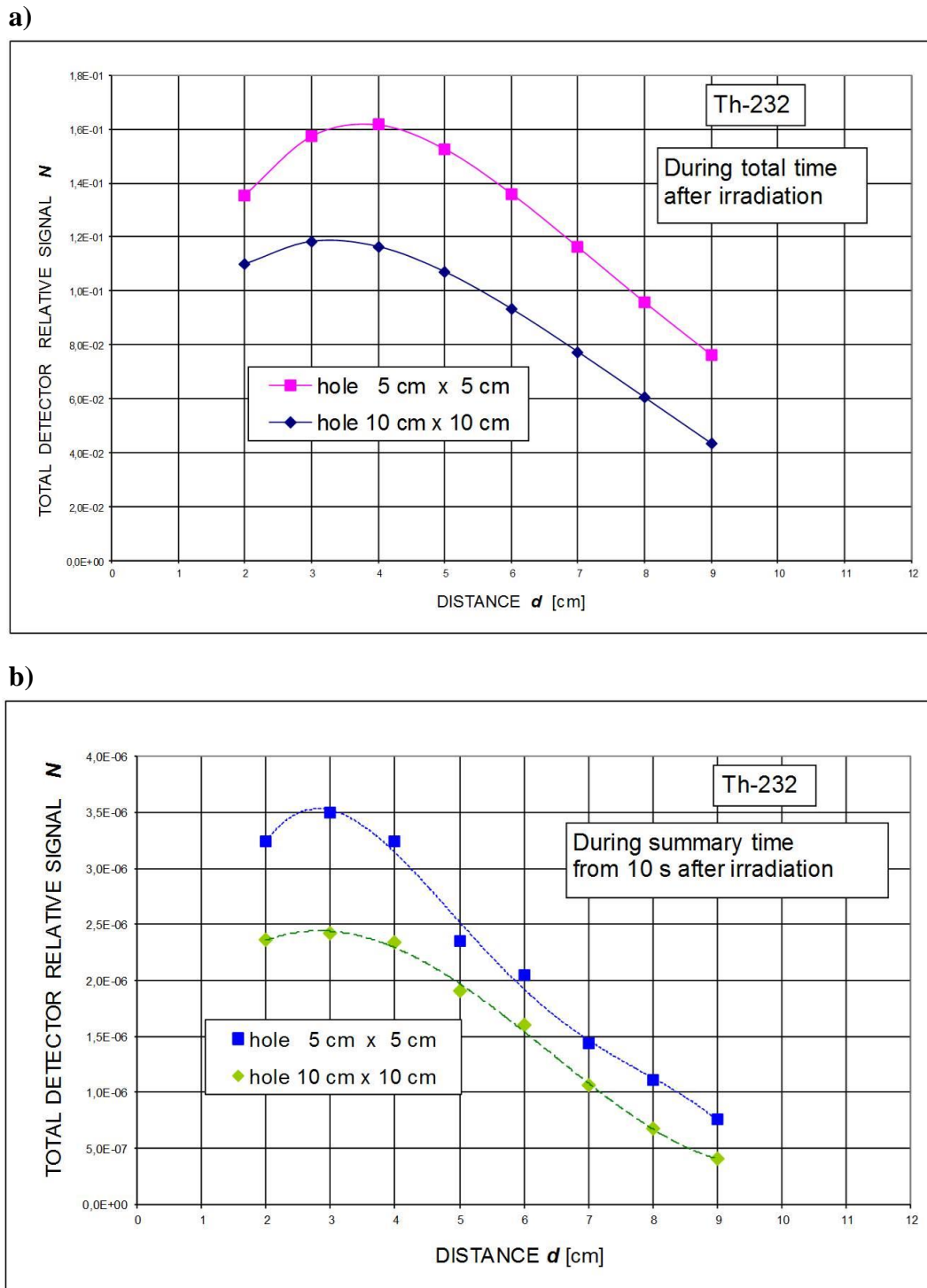
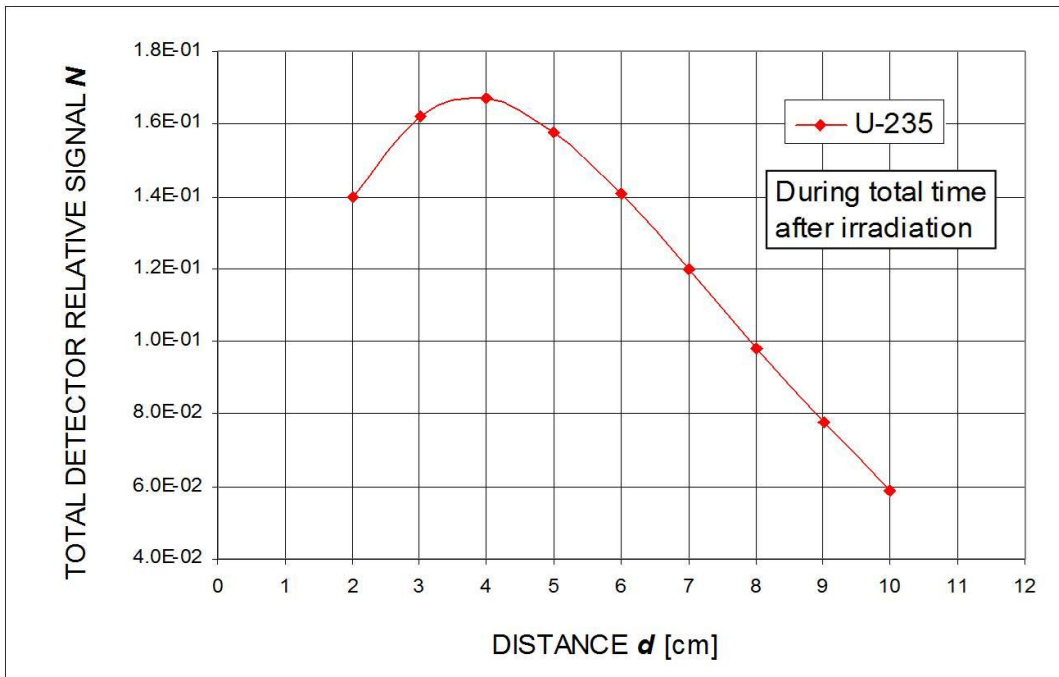


**Fig. 7.** Comparison of the total detector signals from the  $^{232}\text{Th}$  sample as a function of the position  $d$  of the detectors while using different sizes of the central hole for the pneumatic transport. Summary signal integrated over a) the total time, b) the time from 10 s after irradiation.

a)



b)

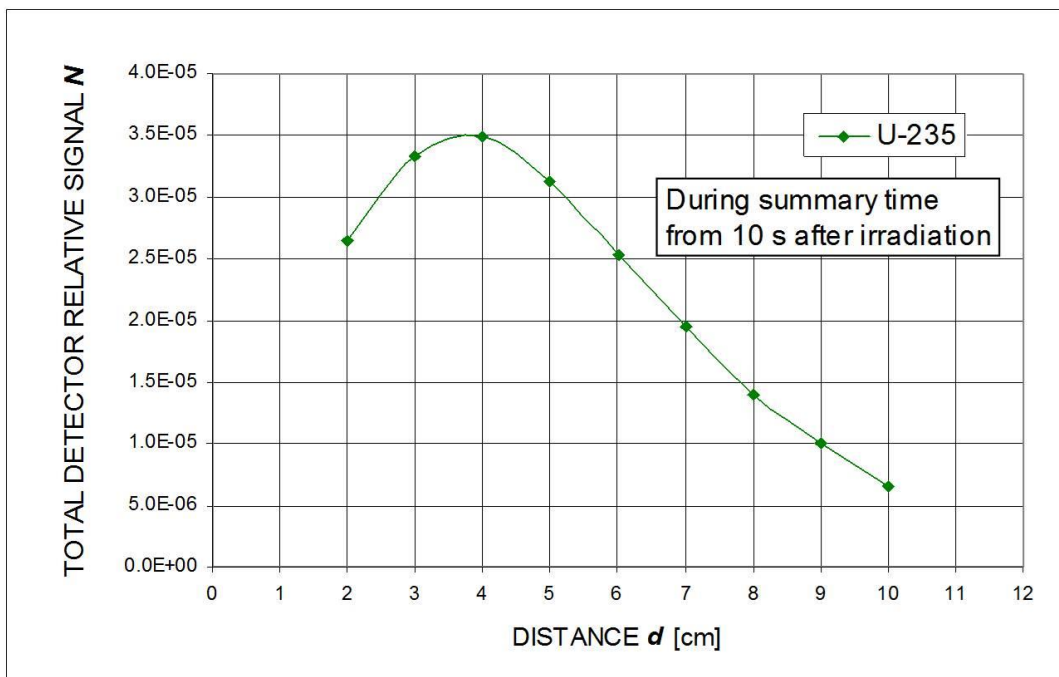
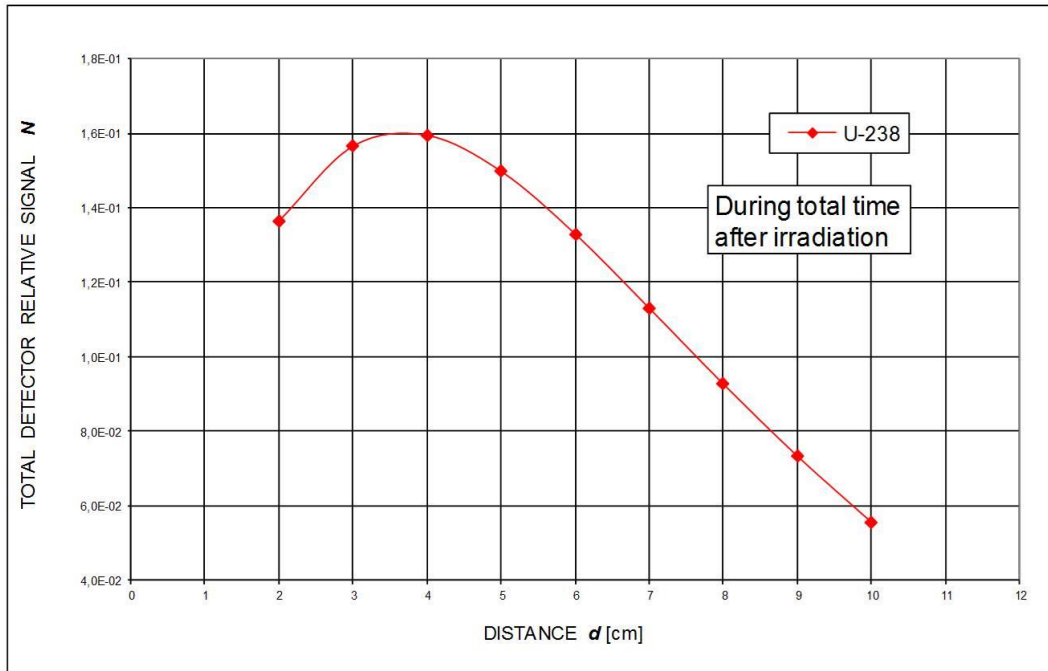


**Fig. 8.** Total detector signals from the  $^{235}\text{U}$  sample as a function of the position  $d$  of the detectors, integrated over a) the total time, b) the time from 10 s after irradiation.  $5 \times 5 \text{ cm}^2$  central hole for the pneumatic transport.

a)



b)

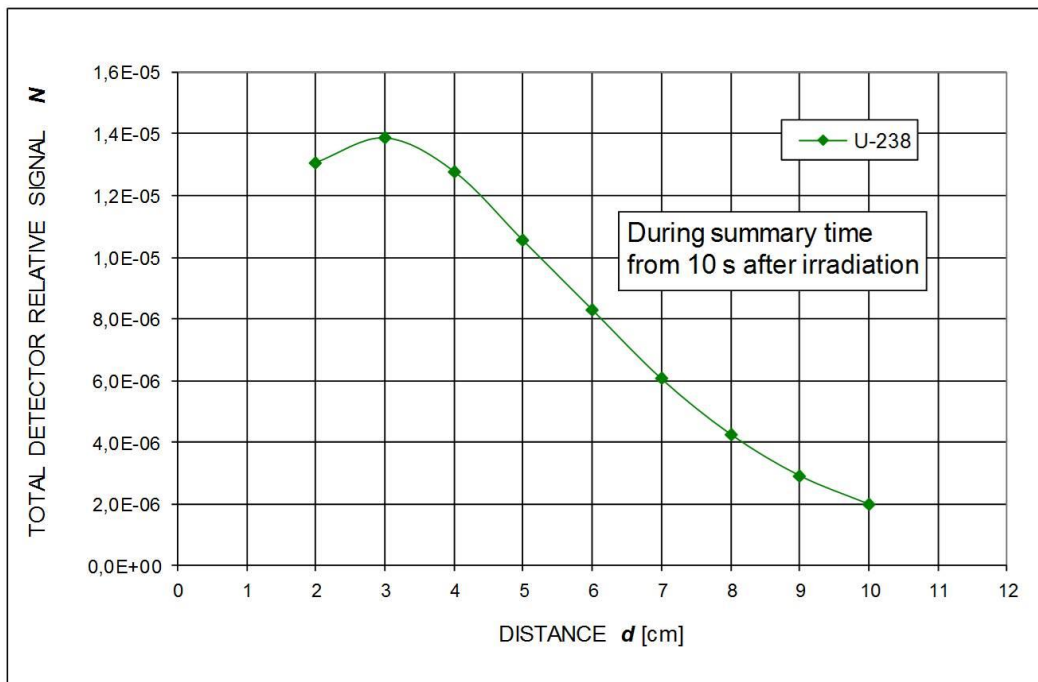


**Fig. 9.** Total detector signals from the  $^{238}\text{U}$  sample as a function of the position  $d$  of the detectors, integrated over a) the total time, b) the time from 10 s after irradiation.  $5 \times 5 \text{ cm}^2$  central hole for the pneumatic transport.

From the results drawn in Figs. 7 to 9, it is visible that maximum efficiency of the measuring device occurs when the  $^3\text{He}$  detectors are placed about 3÷4 cm from the inner interface boundary of polyethylene. It depends slightly on the isotope that emits delayed neutrons and on the moment after irradiation when the measurement starts. A final decision will be also influenced by some technical solutions.

### 3.4. Thickness of the moderator layer

An optimum thickness of the polyethylene moderator layer should be defined. The amount of polyethylene behind the detectors (while looking from the centre) must not be too small if it has to take a significant participation in moderating and reflecting neutrons. On the other hand, some parts of the layer too distant are useless as they do not gain the thermal neutron flux at the detectors and enlarge unnecessary amount of the material, which enlarges a total mass of the device and gives no profit. Monte Carlo simulations of the detector response have been performed varying the width of the polyethylene layer from 6 to 13.5 cm. The total size of the inner polyethylene part of the device changes then from  $21 \times 21 \times 33 \text{ cm}^3$  up to  $36 \times 36 \times 48 \text{ cm}^3$  (cf. Fig. 10). The results of the simulations are presented in Fig. 11.

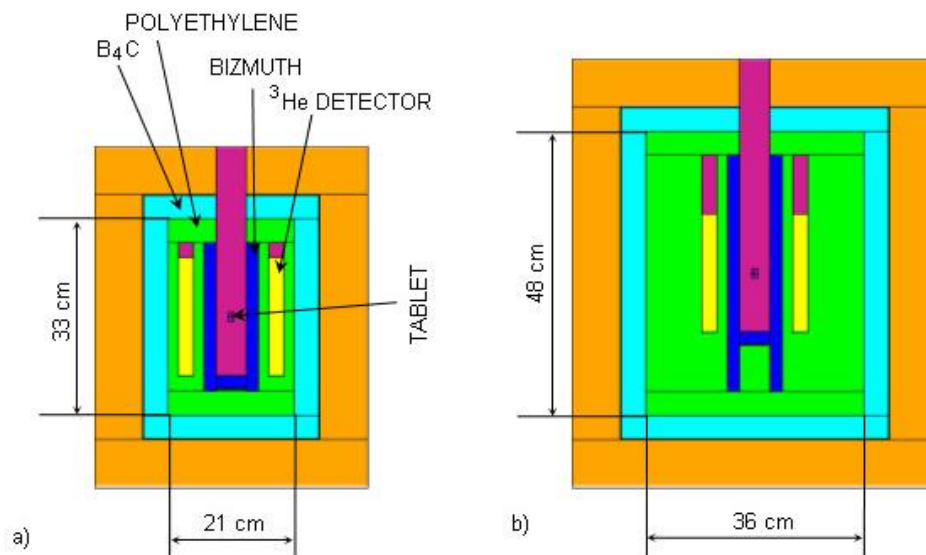


**Fig. 10.** Variation of the thickness  $w$  of the polyethylene moderator:  
a) the smallest and b) the largest investigated sizes (vertical cross section of the device).



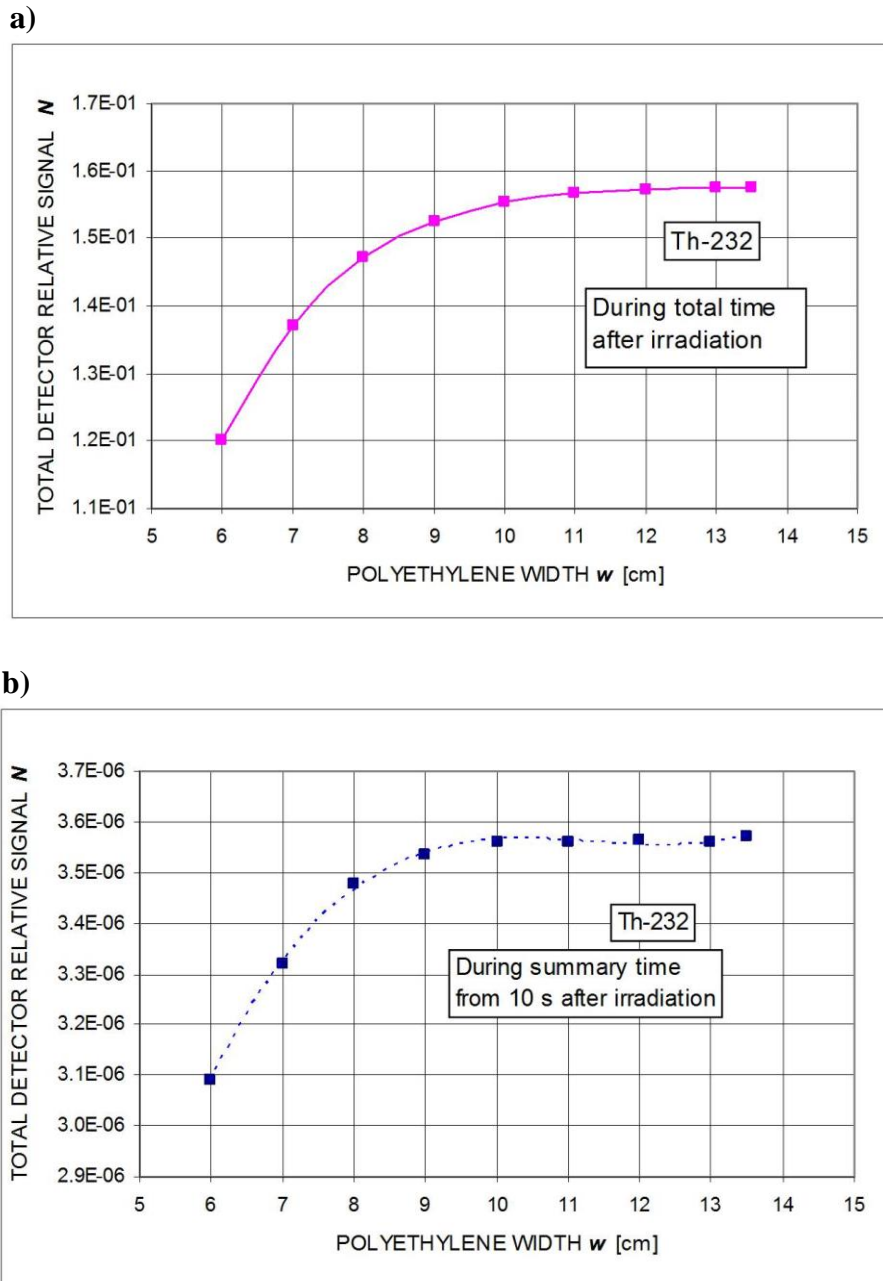


**Fig. 11.** Dependence of the total detector signal on the width  $w$  of the moderator layer, integrated over a) the total time, b) the time from 10 s after irradiation of the  $^{232}\text{Th}$  sample.

Plots in Figs. 11a and 11b show that enlargement of the moderator layer width over 12 cm does not increase the detector signal.

#### 4. Conclusions: Recommendations for a technical design of the measuring chamber

Sizes of important parts of the measuring chamber have been optimized to maximize the neutron detection efficiency. The delayed neutron transport from irradiated samples of

fissionable materials has been modeled with the Monte Carlo method. A detector response has been found as a function of its position in the neutron moderating layer of polyethylene and as a function of this layer width. Three fissionable materials ( $^{235}\text{U}$ ,  $^{238}\text{U}$ ,  $^{232}\text{Th}$ ) have been considered. A sufficient width of the moderator layer has been estimated to 12 cm. An optimum distance of detectors from the inner boundary of the moderator has been found as 3÷4 cm.

General external dimensions of the device are:

square horizontal size  $58 \times 58 \text{ cm}^2$ , height 74 cm.

Hole for the pneumatic transport:  $6 \times 6 \text{ cm}^2$ .

Consecutive layers (from the inner hole towards outside):

Bismuth: 2 cm,

Polyethylene (moderator): 12 cm,

$\text{B}_4\text{C}$  (absorber): 3.8 cm,

Cadmium (absorber): 0.2 cm,

Polyethylene (external protection): 8 cm.

$^3\text{He}$  neutron detectors:

12 pcs., 1" diameter, 30 cm length (25 cm active), 5 atm. pressure.

## Acknowledgment

The authors thank MSc. Andrzej Drabina for his participation in Monte Carlo modelling of the delayed neutron transport performed to optimize design of the DET-12 device.

## References

- [1] K. S. Krane: *Introductory Nuclear Physics*. Wiley, 1988.
- [2] G. R. Keepin, T. F. Wiemett, R. K. Zeigler: *Delayed neutrons from fissionable isotopes of uranium, plutonium, and thorium*. Phys. Rev. **107** (1957) 1044-1049.
- [3] G.D. Spriggs, J. Campbell and V.M. Piksaikin: *An 8-group delayed neutron model based on a consistent set of half-lives*. Progr. Nucl. Energy **41** (2002) 223-251.
- [4] O. N. Jarvis, E. W. Clipsham, M. A. Hone, B. J. Laundy, M. Piullon, M. Rapisarda, G. Sadler, P. van Belle, K. A. Verschuur: *Use of activation techniques for the measurement of neutron yields from deuterium plasmas at the Joint European Torus*. Fusion Technol. **20** (1991) 265-284.
- [5] R. A. Forrest: *ITER, IFMIF and the role of nuclear data*. Proc. of the enlargement workshop "NEMEA-3 – Neutron Measurements, Evaluations and Applications", 25–28 October 2006, Borovets, Bulgaria. Edit. A. J. M. Plompen, EUR Report 22794 EN, 2007, p.19-24.
- [6] A. J. Koning, R. A. Forrest, M. Kellett, R. Mills, H. Henriksson, Y. Rugama: *The JEFF-3.1 Nuclear data library*. JEFF Report 21, 2006.

- [7] A. J. Koning: *The current status and new directions of the JEFF project*. Proc. of the enlargement workshop “NEMEA-3 – Neutron Measurements, Evaluations and Applications”, 25–28 October 2006, Borovets, Bulgaria. Edit. A. J. M. Plompen, EUR Report 22794 EN, 2007, p.25-30.
- [8] O. N. Jarvis et al.: *Time-integrated yield neutron monitor for JET*. AERE Harwell, 1982.
- [9] H. Tourwe et al.: *Delayed neutron counting system for JET plasma neutron yields diagnostics*, in “Reactor Dosimetry”, Springer Netherlands, 1985, p.309-315, doi: 10.1007/978-94-009-5378-9\_30 .
- [10] P. van Belle et al.: *Calibration of the JET neutron yield monitors using delayed neutrons counting technique*. Rev. Sci. Instr. **61** (1990) 3178-3180, doi: 10.1063/1.1141679 .
- [11] O. N. Jarvis: *Neutron measurement techniques for tokamak plasmas*. Plasma Phys. Control. Fusion, **36** (1994) 209-244, [doi:10.1088/0741-3335/36/2/002](https://doi.org/10.1088/0741-3335/36/2/002) .
- [12] D. J. Loaiza: *High-efficiency  $^3\text{He}$  proportional counter for the detection of delayed neutrons*. Nucl. Instrum. Meth. **A 422** (1999) 43-46.
- [13] X-5 Monte Carlo Team: *MCNP – A General Monte Carlo N-Particle Transport Code. Version 5*. Los Alamos National Laboratory, rept. LA-UR-03-1987 (2003/2008).
- [14] D. Pelowitz (Editor): *MCNPX User’s Manual Version 2.5.0*. Los Alamos National Laboratory, rept. LA-CP-05-0369 (2005).